

Direct characterization of coherence of quantum detectors by sequential measurements

Liang Xu^{a,b,c,d,e,†} Huichao Xu^{a,b,c,d,f,†} Jie Xie^{a,b,c,d} Hui Li^{a,b,c,d} Lin Zhou^{a,b,c,d} Feixiang Xu^{a,b,c,d} and Lijian Zhang^{a,b,c,d,*}

^aNanjing University, College of Engineering and Applied Sciences, Nanjing, China

^bNanjing University, Collaborative Innovation Center of Advanced Microstructures, Nanjing, China

^cNanjing University, National Laboratory of Solid State Microstructures, Nanjing, China

^dNanjing University, Key Laboratory of Intelligent Optical Sensing and Manipulation, Nanjing, China

^eResearch Center for Quantum Sensing, Zhejiang Laboratory, Hangzhou, China

^fPurple Mountain Laboratories, Nanjing, China

Abstract. The quantum properties of quantum measurements are indispensable resources in quantum information processing and have drawn extensive research interest. The conventional approach to revealing quantum properties relies on the reconstruction of entire measurement operators by quantum detector tomography. However, many specific properties can be determined by a part of the matrix components of the measurement operators, which makes it possible to simplify the characterization process. We propose a general framework to directly obtain individual matrix elements of the measurement operators by sequentially measuring two noncompatible observables. This method allows us to circumvent the complete tomography of the quantum measurement and extract the required information. We experimentally implement this scheme to monitor the coherent evolution of a general quantum measurement by determining the off-diagonal matrix elements. The investigation of the measurement precision indicates the good feasibility of our protocol for arbitrary quantum measurements. Our results pave the way for revealing the quantum properties of quantum measurements by selectively determining the matrix components of the measurement operators.

Keywords: direct tomography; quantum measurement; weak measurement; sequential measurement; coherence.

Received Sep. 3, 2021; revised manuscript received Oct. 28, 2021; accepted for publication Nov. 4, 2021; published online Nov. 29, 2021.

© The Authors. Published by SPIE and CLP under a Creative Commons Attribution 4.0 International License. Distribution or reproduction of this work in whole or in part requires full attribution of the original publication, including its DOI.

[DOI: [10.1117/1.AP.3.6.066001](https://doi.org/10.1117/1.AP.3.6.066001)]

1 Introduction

The quantum properties of quantum measurements have been widely regarded as an essential resource for the preparation of quantum states,^{1–3} achieving the advantages of quantum technologies,^{4–7} as well as the study of fundamental quantum theories.^{8–15} The time-reversal approach allows for the investigation of the properties of quantum measurements qualitatively from the perspective of quantum states.^{16–18} In addition, the quantum resource theories for quantification of quantum properties of quantum measurements have been developed very recently^{19–22} and have been applied to investigate coherence of quantum-optical detectors.²³ Thus developing efficient approaches to

characterize the quantum properties of quantum measurements is important for both the fundamental investigations and practical applications.

A general quantum measurement and all its properties can be completely determined by the positive operator-valued measure (POVM) $\{\hat{\Pi}_l\}$, in which the element $\hat{\Pi}_l$ denotes the measurement operator corresponding to the outcome l . Several approaches have been developed to determine the unknown POVM,^{24–27} of which the most representative is quantum detector tomography (QDT).²⁴ In QDT, a set of probe states $\{\rho^{(m)}\}$ are prepared to input the unknown measurement apparatus, and the probability of obtaining the outcome l is given by $p_l^{(m)} = \text{Tr}(\rho^{(m)}\hat{\Pi}_l)$. Provided that the input states are informationally complete for the tomography, the POVM $\{\hat{\Pi}_l\}$ can be reconstructed by minimizing the gap between the theoretical calculation and the experimental results. To date, QDT has achieved great success in characterizing a variety of quantum detectors, including

*Address all correspondence to Lijian Zhang, lijian.zhang@nju.edu.cn

[†]These authors contributed equally to this work.

avalanche photodiodes,²⁸ time-multiplexed photon-number-resolving detectors,^{24,29,30} transition edge sensors,³¹ and superconducting nanowire detectors.³² As the quantum detectors become increasingly complicated, the standard QDT is confronted with the experimental and computational challenges, which prompts the exploration of some helpful shortcuts. For example, the determination of a few key parameters that describe the quantum detectors makes it possible to largely reduce the characterization complexity.³³ The quantum detectors can also be self-tested with certain quantum states in the absence of prior knowledge of the apparatus.^{34–37} The emerging data-pattern approach realizes the operational tomography of quantum states through fitting the detector response, which is robust to imperfections of the experimental setup.^{38,39}

Though QDT is a generic protocol to acquire entire measurement operators, it does not have the direct access to the single-matrix components of the measurement operator. The complexity of the reconstruction algorithm in QDT increases dramatically with the increase of the dimensions of the quantum system (QS). Typically, tomography of full measurement operator is considered as the prerequisite for characterizing the properties of quantum measurements.²³ However, in some situations, the complete determination of the measurement operator is not necessary to fulfil specific tasks, which makes it possible to simplify the characterization process. For example, if the input state is known to lie in the subspace of the QS, it only requires the corresponding matrix components of the measurement operators to predict the probability of outcomes.^{29,40,41} In particular, the coherence of a quantum measurement is largely determined by the off-diagonal matrix components of its measurement operators in certain bases.²³

Recently, Lundeen et al.⁴² proposed a method to directly measure the probability amplitudes of the wavefunction using the formalism of the weak measurement and weak values. This method, known as direct quantum state tomography, opens up a new avenue for quantum tomography technique. The direct tomography (DT) protocol has been extensively studied and the scope of its application is expanded to high-dimensional states,^{43–51} mixed states^{52–56} and entangled states,^{57,58} quantum processes,⁵⁹ and quantum measurements.⁶⁰ The development of the DT theory from the original weak-coupling approximation to the rigorous validation with the arbitrary coupling strength ensures the accuracy and simultaneously improves the precision.^{61–68} Moreover, direct state tomography allows the direct measurement of any single-matrix entry of the density matrix, which has provided an exponential reduction of measurement complexity compared to standard quantum state tomography in determining a sparse multiparticle state.^{53–56,69} Recent work has extended the idea to realize

the direct characterization of full measurement operators, based on weak values, showing the potential advantages over QDT in operational and computational complexity.⁶⁰ In view of the unique advantages of the DT, it is expected that the generalization of the DT scheme for directly characterizing the matrix components of measurement operators allows for the extraction of the properties of the quantum measurement in a more efficient way.

In this paper, we propose a framework to directly characterize the individual matrix components of the measurement operators by sequentially measuring two noncompatible observables with two independent meter states (MSs). In the following, the unknown quantum detector performs measurement on the QS. The specific matrix entry of the measurement operator can be extracted from the collective measurements on the MSs when the corresponding outcomes of the quantum detector are obtained. Our procedure is rigorously valid with the arbitrary non-zero coupling strength. The investigations of the measurement precision indicate the good feasibility of our scheme to characterize arbitrary quantum measurement. We experimentally demonstrate our protocol to monitor the evolution of coherence of the quantum measurement in two different situations, the dephasing and the phase rotation, by characterizing the associated off-diagonal matrix components. Our results show the great potential of the DT for capturing the quantum properties of the quantum measurement through partial determination of the measurement operators.

2 Theoretical Framework

2.1 Directly Determining the Matrix Components of the Measurement Operators

The schematic diagram for direct characterization of the matrix components of the POVM is shown in Fig. 1. We represent the POVM $\{\hat{\Pi}_l\}$ acting on the d -dimensional QS with the orthogonal basis $\{|a_j\rangle\}$ (\mathcal{A}), and the matrix entry of the measurement operator $\hat{\Pi}_l$ is given by $E_{a_j a_k}^{(l)} = \langle a_j | \hat{\Pi}_l | a_k \rangle$. If $j = k$, $E_{a_j a_k}^{(l)}$ corresponds to the diagonal matrix entry, which can be easily determined by inputting a preselected QS state $\rho_s^{(j)} = |a_j\rangle\langle a_j|$ to the quantum detector and collecting the probability $p_l = \langle a_j | \hat{\Pi}_l | a_j \rangle$ of obtaining the outcome l . By contrast, the off-diagonal matrix entry $E_{a_j a_k}^{(l)}$ ($j \neq k$), generally a complex number, is related to the coherence of the operator and usually indirectly reconstructed in the conventional QDT. In order to directly measure $E_{a_j a_k}^{(l)}$ ($j \neq k$), we perform the sequential measurement of the observables $\hat{O}_B = \hat{I} - 2|b_0\rangle\langle b_0|$ (note that $|b_0\rangle$

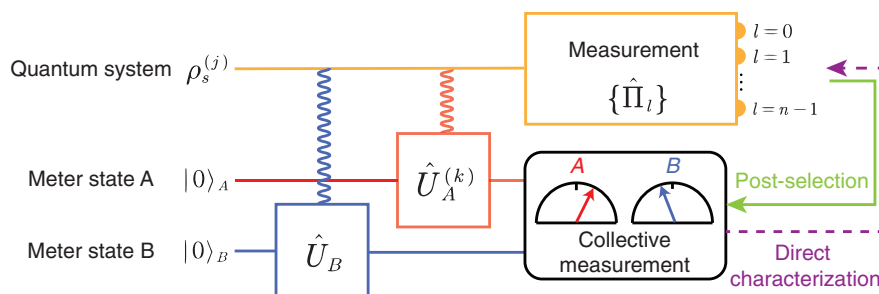


Fig. 1 The schematic diagram for direct characterization of the matrix components of the POVM $\{\hat{\Pi}_l\}$.

is a state vector which is a superposition of all the base states in basis \mathcal{A} with the equal probability amplitudes, i.e., $|b_0\rangle \propto \sum_j |a_j\rangle$ and $\hat{O}_A^{(k)} = \hat{I} - 2|a_k\rangle\langle a_k|$ on the initial state $\rho_s^{(j)}$ with two independent two-dimensional MSs initialized as $|0\rangle_B$ and $|0\rangle_A$, respectively. The measurement of the observable \hat{O} (generally referring to the observable \hat{O}_B or $\hat{O}_A^{(k)}$) is implemented by coupling the QS with the MS under the Hamiltonian $\hat{H} = g\delta(t-t_0)\hat{O} \otimes \hat{\sigma}_y$, in which g is the coupling strength and $\hat{\sigma}_y = i(|1\rangle\langle 0| - |0\rangle\langle 1|)$ is the observable of the MS. Since the observables \hat{O}_B and $\hat{O}_A^{(k)}$ do not commute, the measurement has to be performed in a particular order.

The sequential measurement process can be described by the unitary evolution of the system-MS $\rho_{sm} = \rho_s^{(j)} \otimes \rho_{m,B} \otimes \rho_{m,A}$ with the first transformation,

$$\hat{U}_B = \exp(-ig_B \hat{O}_B \otimes \hat{\sigma}_{y,B} \otimes \hat{I}_A), \quad (1)$$

and the second transformation,

$$\hat{U}_A^{(k)} = \exp(-ig_A \hat{O}_A^{(k)} \otimes \hat{I}_B \otimes \hat{\sigma}_{y,A}), \quad (2)$$

leading to the joint state,

$$\rho_J = \hat{U}_A^{(k)} \hat{U}_B \rho_{sm} \hat{U}_B^\dagger \hat{U}_A^{(k)\dagger}. \quad (3)$$

Then the unknown quantum detector to be characterized performs the postselection measurement $\{\hat{\Pi}_l\}$ on the QS. Depending on the measurement outcome l , the surviving final MS is given by $\rho'_{m,A,B} = \text{Tr}_s(\hat{\Pi}_l \otimes \hat{I}_B \otimes \hat{I}_A \rho_J) / p_f$, in which $\text{Tr}_s(\cdot)$ denotes the partial trace operation on the QS, and $p_f = \text{Tr}(\hat{\Pi}_l \otimes \hat{I}_B \otimes \hat{I}_A \rho_J)$ is the probability for getting the outcome l .

The matrix entry $E_{a_j a_k}^{(l)}$ is related to the average value of the observables \hat{O}_B and $\hat{O}_A^{(k)}$ by

$$E_{a_j a_k}^{(l)} = \frac{d}{4} \text{Tr} \left[\hat{\Pi}_l (\hat{I} - \hat{O}_A^{(k)}) (\hat{I} - \hat{O}_B) \rho_s^{(j)} \right]. \quad (4)$$

Both of the observables \hat{O}_B and $\hat{O}_A^{(k)}$ are designed to satisfy $\hat{O}^2 = \hat{I}$ so that the unitary is exactly expanded as $\hat{U} = \exp(-ig\hat{O} \otimes \hat{\sigma}_y) = \cos g \hat{I} \otimes \hat{I} - i \sin g \hat{O} \otimes \hat{\sigma}_y$. The right side of Eq. (4) can be extracted by the joint measurement of post-selected MS $\rho'_{m,A,B}$ with the observables

$$\hat{P} = \sqrt{d} \left(\frac{\hat{I} + \hat{\sigma}_z}{4 \cos^2 g} - \frac{\hat{\sigma}_x}{4 \sin g \cos g} \right),$$

$$\hat{Q} = -\frac{\sqrt{d} \hat{\sigma}_y}{4 \sin g \cos g}, \quad (5)$$

each in the subsystems A and B . By defining the joint observables of MSs A and B as $\hat{R}_{B,A} = \hat{P}_B \hat{P}_A - \hat{Q}_B \hat{Q}_A$ and $\hat{T}_{B,A} = \hat{P}_B \hat{Q}_A + \hat{Q}_B \hat{P}_A$, we obtain the real and the imaginary parts of $E_{a_j a_k}^{(l)}$:

$$\text{Re}[E_{a_j a_k}^{(l)}] = \text{Tr}(\hat{\Pi}_l \otimes \hat{R}_{B,A} \rho_J),$$

$$\text{Im}[E_{a_j a_k}^{(l)}] = \text{Tr}(\hat{\Pi}_l \otimes \hat{T}_{B,A} \rho_J). \quad (6)$$

Here, the subscripts of the coupling strength g and the Pauli operators coincide with those of the operators \hat{P} and \hat{Q} . For the sake of convenience, $g_A = g_B = g$ in the rest of this article.

2.2 Precision Analysis on Directly Characterizing the Matrix Components of the Measurement Operators

The accuracy and the precision are two essential indicators to evaluate a measurement scheme. There are no systematic errors in our protocol, since the derivation is rigorous for the arbitrary coupling strength g . According to previous studies, the precision of the DT applied to the quantum states is sensitive to both the coupling strength and the unknown states.⁷⁰ The increase of the coupling strength is beneficial to improving the precision.⁶²⁻⁶⁸ When the unknown state approaches being orthogonal to the postselected state, the DT protocol is prone to large statistical errors and is therefore highly inefficient.^{70,71} Here, we theoretically investigate the precision of the DT protocol applied to the quantum measurement to verify the feasibility of our protocol.

Given that the real and the imaginary parts of the matrix components are independently measured, we quantify the measurement precision with the total variance $\Delta^2 E_{a_k a_j}^{(l)} = \Delta^2 \text{Re}[E_{a_k a_j}^{(l)}] + \Delta^2 \text{Im}[E_{a_k a_j}^{(l)}]$. According to Eq. (6), the variance can be derived by

$$\Delta^2 E_{a_k a_j}^{(l)} = \langle \Delta^2 \hat{R}_{B,A} \rangle_f + \langle \Delta^2 \hat{T}_{B,A} \rangle_f, \quad (7)$$

where $\langle \Delta^2 \hat{M} \rangle_f = \text{Tr}(\hat{\Pi}_l \hat{M}^2 \rho_J) - [\text{Tr}(\hat{\Pi}_l \hat{M} \rho_J)]^2$. Since the operators $\hat{R}_{B,A}$ and $\hat{T}_{B,A}$ are usually hard to experimentally construct, an alternative is to infer the expected values of $\hat{R}_{B,A}$ and $\hat{T}_{B,A}$ as well as their squares, from the complete measurement results of the MSs B and A , each projected to the mutually unbiased bases, i.e., $\{|0\rangle, |1\rangle\}$, $\{|+\rangle, |-\rangle\}$, $\{|\heartsuit\rangle, |\spadesuit\rangle\}$ with $|\pm\rangle = (|0\rangle \pm |1\rangle)/\sqrt{2}$ and $|\heartsuit\rangle, |\spadesuit\rangle = (|0\rangle \pm i|1\rangle)/\sqrt{2}$. The obtained probability distribution is represented by $\{W_{mn}\}$, where m and n label the projective states $|m_B\rangle$ and $|m_A\rangle$ of the MSs B and A , respectively. The experimental variance can be obtained from $\{W_{mn}\}$ with the error transfer formula

$$\Delta^2 E_{a_k a_j}^{(l)} = \sum_{m,n} \left| \frac{\partial E_{a_k a_j}^{(l)}}{\partial W_{mn}} \right|^2 \delta^2 W_{mn}. \quad (8)$$

Consider that N particles are used for one measurement of W_{mn} . The variance of the probability is approximated as $\delta^2 W_{mn} \approx W_{mn}/N$ in the large N limit due to the Poissonian statistic.

As a demonstration, we theoretically derive the precision of directly measuring the off-diagonal matrix entry $E_{1,0}(\theta)$ of a general measurement operator for a two-dimensional QS as follows:

$$\hat{\Pi}(\theta) = \eta \begin{pmatrix} \cos^2 \theta & E_{0,1}(\theta) \\ E_{1,0}(\theta) & \sin^2 \theta \end{pmatrix}, \quad (9)$$

with different coupling strength g . According to Eq. (8), the variance of the off-diagonal matrix entry $E_{1,0}(\theta)$ is given by

$$\Delta^2 E_{1,0}(\theta) = \frac{(\sin^2 \theta + \sin^2 g)(1 + 2 \sin^2 g)}{\eta N \sin^4(2g)}. \quad (10)$$

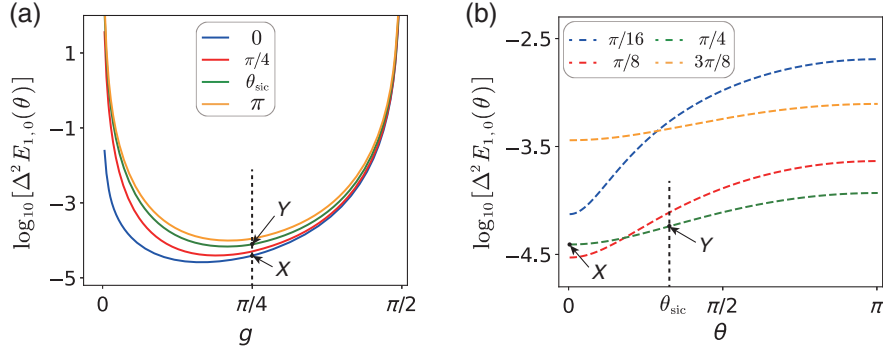


Fig. 2 The measurement precision of the off-diagonal matrix element $E_{1,0}(\theta)$ of the measurement operator $\hat{\Pi}(\theta)$ in a two-dimensional QS. (a) The variance of $E_{1,0}(\theta)$ is plotted with different g for four values of $\theta = 0, \pi/4, \theta_{\text{sic}}, \pi$ with $\theta_{\text{sic}} = \arccos(1/\sqrt{3})$. (b) The variance of $E_{1,0}(\theta)$ changes with different parameters θ for the coupling strength $g = \pi/16, \pi/8, \pi/4, 3\pi/8$. Here, we take $\eta = 1/2$ and $N = 12,790$ to coincide with our experimental conditions. The points X and Y refer to the precision of directly measuring the off-diagonal matrix entry of the two-dimensional symmetric informationally complete positive operator-valued measure (SIC POVM) with the coupling strength $g = \pi/4$.

In Fig. 2(a), we show how the variance of $E_{1,0}(\theta)$ changes with different g for four values of θ . We find that the statistical errors $\Delta^2 E_{1,0}(\theta)$ become large with a small coupling strength ($g \rightarrow 0$ or $g \rightarrow \pi/2$), whereas the strong coupling strength ($g \rightarrow \pi/4$) significantly decreases the variance to $\Delta^2 E_{1,0}(\theta)|_{g=\pi/4} = (1 + 2 \sin^2 \theta)/(\eta N)$. We also compare the characterization precision of $E_{1,0}(\theta)$ associated with different POVM parameters θ in Fig. 2(b). The statistical errors $\Delta^2 E_{1,0}(\theta)$ remain finite over all θ indicating that our protocol is applicable to characterize the arbitrary POVM of a two-dimensional QS. In addition, the variance $\Delta^2 E_{1,0}(\theta)$ is related to the parameter θ but does not depend on the value of $E_{1,0}(\theta)$. This implies that the change of the off-diagonal matrix components of the measurement operator, such as the dephasing and the phase rotation process, will not affect the characterization precision. We note that the choice of the sequential observables \hat{O}_B and $\hat{O}_A^{(k)}$ is indeed not unique. How to choose the optimal observables of the QS to achieve the best characterization precision remains an open question in the field of DT. If the sequential observables of the QS are changed, the collective observables $\hat{R}_{B,A}$ and $\hat{T}_{B,A}$ of the MSs should also be changed correspondingly, and the method to reveal the matrix components $E_{a_j a_k}^{(l)}$ may be more involved.

It has been shown that the completeness condition of the POVM $\{\hat{\Pi}_l\}$, i.e., $\sum_l \hat{\Pi}_l = \hat{I}$, can be used to improve the precision of direct QDT.⁶⁰ In the following, we prove that the same condition is also helpful to improve the precision in the direct characterization of $E_{a_j a_k}^{(l)}$ ($j \neq k$). Since the real part of the components $E_{a_j a_k}^{(l)}$ satisfies $\sum_l \text{Re}[E_{a_j a_k}^{(l)}] = 0$, the value of $\text{Re}[E_{a_j a_k}^{(l)}]$ can be not only obtained by the direct measurement but also inferred from the components of other POVM elements $\text{Re}[E_{a_j a_k}^{(u)}]$ ($u \neq l$) by $\text{Re}[E_{a_j a_k}^{(l)}] = -\sum_{u \neq l} \text{Re}[E_{a_j a_k}^{(u)}]$. The extra information obtained by $\text{Re}[E_{a_j a_k}^{(l)}]$ can be used to improve the measurement precision. To acquire the best precision, we adopt the weighted average of $\text{Re}[E_{a_j a_k}^{(l)}]$ and $\text{Re}[E_{a_j a_k}^{(l)\circ}]$ with the weighting factors w and w° , respectively. The optimal weighting factors satisfy the condition

$$\begin{aligned} w + w^\circ &= 1, \\ w &\propto \frac{1}{\Delta^2 \text{Re}[E_{a_j a_k}^{(l)}]}, \\ w^\circ &\propto \frac{1}{\sum_{u \neq l} \Delta^2 \text{Re}[E_{a_j a_k}^{(u)}]}, \end{aligned} \quad (11)$$

leading to the optimal precision $\Delta^2 \text{Re}[E_{a_j a_k}^{(l)}] = w w^\circ / \sum_u \Delta^2 \text{Re}[E_{a_j a_k}^{(l)}] < \Delta^2 \text{Re}[E_{a_j a_k}^{(l)}]$.

3 Experiment

In the experiment, we apply the DT protocol to characterize the SIC POVM in the polarization degree of freedom (DOF) of photons. Since the coherence between two polarization base states only changes the off-diagonal components of the measurement operators, we demonstrate that the dephasing and the phase rotation of the SIC POVM can be monitored by only characterizing the corresponding matrix components.

The experimental setup is shown in Fig. 3. We refer to the polarization DOF of photons as the QS with the eigenstates $|H\rangle$ and $|V\rangle$. Single photons generated by the spontaneous parametric downconversion pass through the polarizing beam splitter (PBS) and a half-wave plate (HWP) at 45 deg to preselect the QS to $|V\rangle$. The “measurement 1” and “measurement 2” modules implement the measurement of the observables $\hat{O}_B = |D\rangle\langle D| - |A\rangle\langle A|$ and $\hat{O}_A = |H\rangle\langle H| - |V\rangle\langle V|$, where $|D\rangle = (|H\rangle + |V\rangle)/\sqrt{2}$ and $|A\rangle = (|H\rangle - |V\rangle)/\sqrt{2}$.

Here, we take measurement 1 as an example to describe the working principle of the coupling scenario. The HWP at 22.5 deg before the polarizing beam displacer (PBD) transforms the measurement basis $\{|D\rangle, |A\rangle\}$ into $\{|H\rangle, |V\rangle\}$, and the observable $\hat{\sigma}_z = |H\rangle\langle H| - |V\rangle\langle V|$ is measured between the two PBDs. The first PBD converts the DOF of the QS into the optical path, with $|H\rangle \rightarrow |0\rangle$ and $|V\rangle \rightarrow |1\rangle$. The polarization of photons in each path initialized to $|H\rangle$ is used as the MS. Two HWPs are arranged in parallel, each on different paths, and are rotated, respectively, to $g/2$ and $-g/2$, to realize the

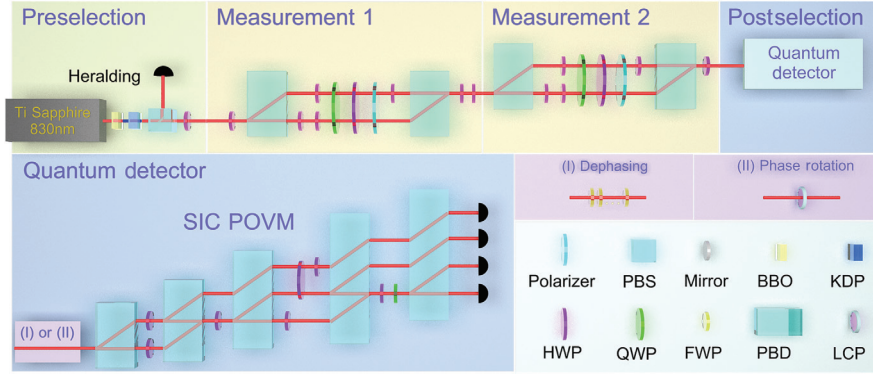


Fig. 3 The experimental setup for characterization of the evolution of the quantum measurement. The pulse laser at 830 nm enters a BBO crystal for the upconversion. The generated photons at 415 nm get through a KDP crystal for the spontaneous parametric downconversion, which simultaneously produces a pair of photons. The single photon is heralded by detecting the other one of the pair. The measurement 1 and measurement 2 modules successively implement the unitary transformation \hat{U}_B and $\hat{U}_A^{(k)}$ as well as the joint measurement on the MSs. In the following, the unknown quantum detector performs the postselection measurement on the polarization DOF of photons. The quantum detector is composed of the operation of polarization evolution, i.e., “(I) dephasing” and “(II) phase rotation” and the SIC POVM realized by the quantum walk. The abbreviations of the equipment are as follows: PBS, polarizing beam splitter; BBO, β -barium borate crystal; KDP, potassium dihydrogen phosphate; HWP, half-wave plate; QWP, quarter-wave plate; PBD, polarizing beam displacer; FWP, full-wave plate; and LCP, liquid-crystal plate.

coupling between the QS and the MS. Afterward, we measure the polarization of photons to extract the information of the MS by a quarter-wave plate (QWP), an HWP, and a polarizer. The photons in two paths that pass through the polarizer recombine at the second PBD and the subsequent two HWPs at 45 deg and 22.5 deg recover the measurement basis to $\{|H\rangle, |V\rangle\}$. A similar setup of measurement 2 performs the measurement of the operator \hat{O}_A . Finally, the photons input the unknown detector for the postselection. By collecting the photons that arrive at the outputs, we obtain the measurement results.

We construct the SIC POVM $\{\hat{\Pi}_l\}$ with $\hat{\Pi}_l = \frac{1}{2}|\psi_l\rangle\langle\psi_l|$ ($l = 1, 2, 3, 4$) and

$$\begin{aligned} |\psi_1\rangle &= |H\rangle, \\ |\psi_2\rangle &= \left(|H\rangle - \sqrt{2}|V\rangle\right) / \sqrt{3}, \\ |\psi_3\rangle &= \left(|H\rangle + \sqrt{2}e^{-i2\pi/3}|V\rangle\right) / \sqrt{3}, \\ |\psi_4\rangle &= \left(|H\rangle + \sqrt{2}e^{i2\pi/3}|V\rangle\right) / \sqrt{3}, \end{aligned} \quad (12)$$

through the quantum walk to perform the postselection measurement of the QS.⁷² The dephasing of the POVM is realized by several full-wave plates (FWPs), which separate the wave packets in polarization states $|H\rangle$ and $|V\rangle$, i.e., $|\varphi(t_H)\rangle$ and $|\varphi(t_V)\rangle$ in the temporal DOF. This separation causes the dephasing of the POVM and the off-diagonal entries $E_{VH}^{(l)}$ are transformed to $E_{VH}^{(l,D)} = E_{VH}^{(l)}\xi$ with the coefficient $\xi = \langle\varphi(t_H)|\varphi(t_V)\rangle$. The derivation of the dephasing process and the calibration of the coefficient ξ are provided in the [Appendix](#). The phase rotation is implemented by the liquid crystal plate (LCP), which imposes a relative phase ϕ_{lc} between $|H\rangle$ and $|V\rangle$.

The operation is equivalent to the unitary evolution $\hat{U}_{lc} = \exp(i\frac{\phi_{lc}}{2}\hat{C})$ of the input state, with $\hat{C} = |H\rangle\langle H| - |V\rangle\langle V|$. When the evolution is inversely performed on the SIC POVM, the non-diagonal elements $E_{VH}^{(l)}$ are transformed to $E_{VH}^{(l,R)} = E_{VH}^{(l)} \exp(-i\phi_{lc})$. The calibration results of the ϕ_{lc} are shown in the [Appendix](#), Sec. 6.2.

4 Results

In Fig. 4, we compare the experimental results of DT with those of the conventional tomography (CT) as well as the ideal SIC POVM during the dephasing and phase rotation process. The detailed information of characterizing the experimental SIC POVM by CT is provided in the [Supplementary Material](#). The results of CT, shown in Fig. 4, are inferred from the experimental SIC POVM and the calibrated coefficient ξ (during the dephasing process) or the phase ϕ_{lc} (during the phase rotation process). As shown in Fig. 4(a), the points in each connecting solid line along the direction of arrows correspond to the relative time delay $\epsilon = 0\lambda, 20\lambda, 40\lambda, 60\lambda, 80\lambda, 120\lambda, 160\lambda, 200\lambda, 240\lambda$. The increase of the relative time delay ϵ between the separated wave packets reduces the overlap of the temporal wavefunction $\xi = \langle\varphi(t_H)|\varphi(t_V)\rangle$, which leads to the dephasing of the quantum measurement. The relation between the relative time delay ϵ and the coefficient ξ is calibrated in Fig. 5(b) of the [Appendix](#), Sec. 6.2. Correspondingly, the modulus of $E_{VH}^{(l,D)}$ gradually approaches 0, implying that the quantum measurement becomes incoherent, i.e., loses the ability of detecting the coherence information of a quantum state.

In Fig. 4(b), we plot $E_{VH}^{(l,R)}$ during the phase-rotation process. The imposed voltage on the LCP is adjusted to obtain $\phi_{lc} = 2\pi/5$ and $4\pi/5$. A HWP at 0 deg is placed before the LCP to obtain $\phi_{lc} = -3\pi/5$ and $-\pi/5$. The rotated points

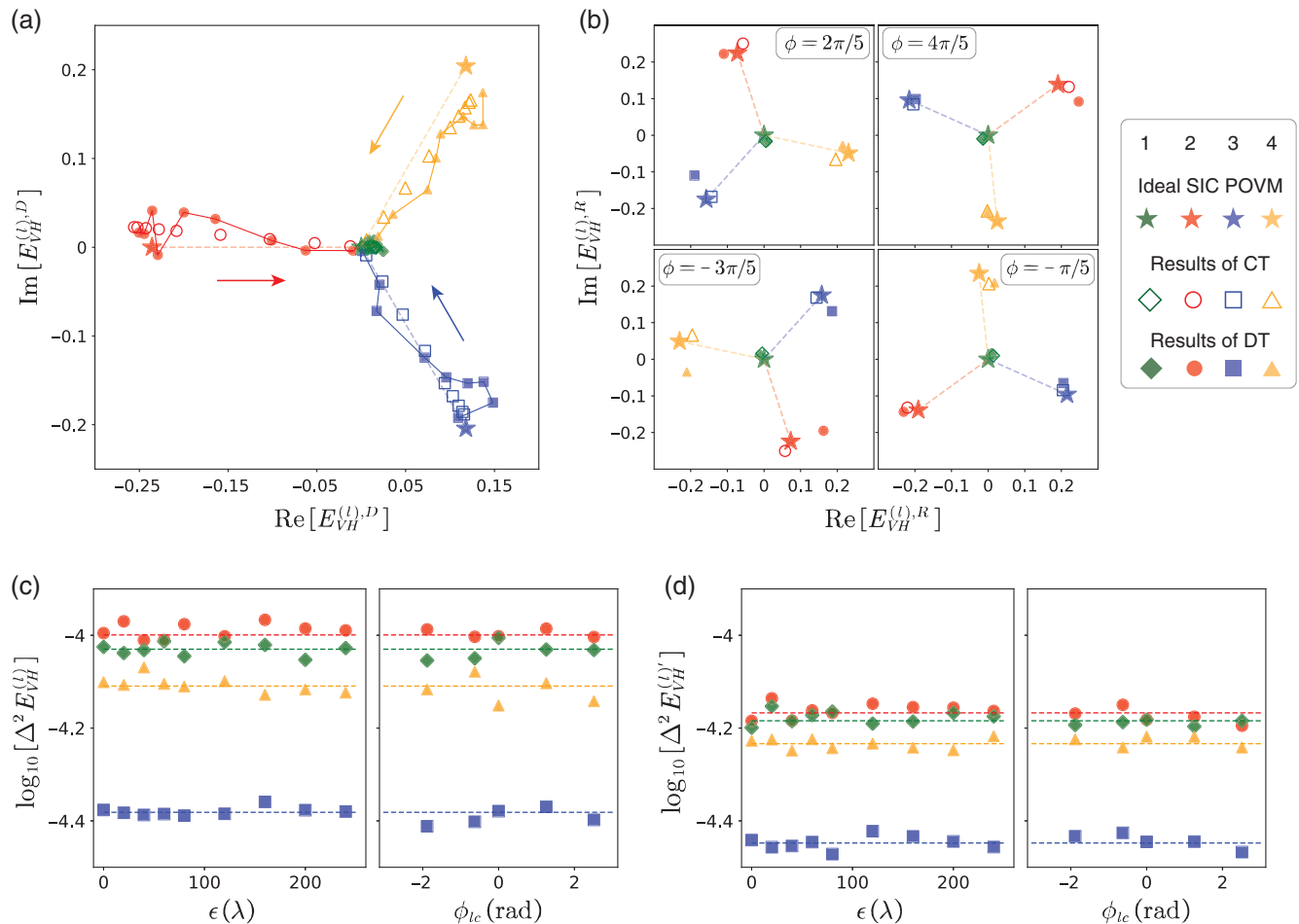


Fig. 4 (a), (b) The real and the imaginary parts of the matrix components $E_{VH}^{(l)}$ are plotted during the dephasing ($E_{VH}^{(l),D}$) and the phase rotation ($E_{VH}^{(l),R}$) of the polarization, respectively. The results of the ideal SIC POVM, the CT, and the DT are represented by the pentagrams, hollow markers, and solid markers, respectively. In panels (a) and (b), we connect each pentagram with the point (0, 0), indicating the evolution path of the ideal SIC POVM during the dephasing process as well as changes of the azimuth angles during the phase rotation process. (c) The statistical errors of the matrix components $E_{VH}^{(l)}$ are provided for both the dephasing and the phase rotation process. (d) The precision of $E_{VH}^{(l)'}$ after using the completeness condition of the POVM. The theoretical precision, represented by the dashed lines in panels (c) and (d), is inferred from the experimental results of CT. The average photon number per unit time for one collective measurement of the MSs is about $N = 12,790$.

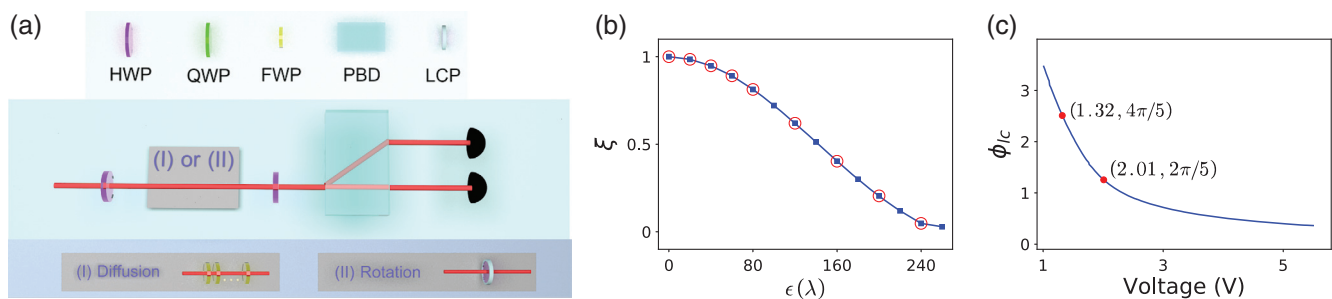


Fig. 5 The calibration of the equipment in the dephasing and the phase rotation process. (a) The calibration setup. (b) The coefficient ξ changes with the time delay ϵ between the wave packets in states $|H\rangle$ and $|V\rangle$. (c) The relative phase ϕ_{lc} between the states $|H\rangle$ and $|V\rangle$ changes with imposed voltage.

representing $E_{VH}^{(l),R}$ in the coordinates of its real and imaginary parts indicate the phase rotation of the quantum measurement. During the phase rotation process, the modulus of $E_{VH}^{(l),R}$ remains unchanged, which indicates that the coherence of the quantum measurement is maintained.

The total noise in the experiment contains the statistical noise and the technical noise. The statistical noise originates from the fluctuations of the input photon numbers per unit time due to the probabilistic generation of single photons, the loss in the channel, and the finite trials of the experiment. The technical noise is caused by the experimental imperfections, e.g., the equipment vibration or the air turbulence. As shown in Figs. 4(a) and 4(b), the experimental results fluctuate around the theoretical predictions due to both the statistical noise and the technical noise. The technical noise can be reduced by isolating the noise source or adopting appropriate signal modulation. The statistical noise determines the ultimate precision that can be achieved for a specific amount of input resources, which is an important metric to evaluate whether a measurement protocol is efficient or not.

The statistical errors of the experimental results are shown in Fig. 4(c). The theoretical precision, represented by dashed lines in Figs. 4(c) and 4(d), is inferred by assuming that the matrix components $E_{VH}^{(l)}$ of the experimental SIC POVM obtained by the CT are directly characterized. As a comparison, we can refer to Fig. 2 for the theoretical precision of the ideal SIC POVM, represented by the points X ($\theta = 0, g = \pi/4$) and Y ($\theta = \arccos(1/\sqrt{3}), g = \pi/4$). Since the experimental SIC POVM deviates from the ideal SIC POVM, the precisions of $l = 2, 3, 4$ do not equate with each other. The experimental precision is obtained from the Monte Carlo simulation based on the experimental probability distribution and the practical photon statistics to eliminate the effect of the technical noise. Our results closely follow the theoretical predictions indicating that the precision of measuring the off-diagonal matrix components of the POVM is immune to the dephasing and phase rotation of the quantum measurement. We can also find that the characterization precision after using the completeness condition in Fig. 4(d) is significantly improved compared to the original precision in Fig. 4(c).

5 Discussion and Conclusion

We have proposed a protocol to directly characterize the individual matrix components of the general POVM, extending the scope of the DT scheme. Our expression is rigorous for the arbitrary coupling strength, which allows us to change the coupling strength to improve the precision and simultaneously maintain the accuracy. The statistical errors are finite over all the choices of the POVM parameter, demonstrating the feasibility of our protocol for the arbitrary POVM. In particular, if the completeness condition of the POVM is appropriately used, the measurement precision can be further improved. Our results indicate that the characterization precision is not affected by the dephasing and phase rotation that only change the off-diagonal matrix components of the measurement operators. Another typical noise is the phase diffusion, meaning that the phase of the quantum measurements randomly jitters. According to the derivations in the paper,⁷³ the phase diffusion decreases the modulus of the off-diagonal matrix components in a similar way to the dephasing in our work. Therefore, it is expected that the precision of our protocol is immune to incoherent noise, such as phase diffusion.

Since some properties of quantum measurements may depend on a part of matrix components of the measurement operators, this protocol allows us to reveal these properties without the full tomography. We experimentally demonstrate that the evolution of the coherence of a quantum measurement can be monitored through determining the off-diagonal matrix components of the measurement operators. Our scheme makes no assumptions about the basis to represent the measurement operators. The choice of the basis depends on the specific conditions or can be optimized according to the purpose of the characterization. Sometimes, the choice of the basis is natural. For example, the photon number basis is typically employed to represent the measurement operators of photodetectors.^{24,28–30,40} In some cases, we aim to acquire the response of the quantum measurements to specific properties of quantum states in which the basis is specified by that used to define the property. Additionally, the basis can be optimized to seek the best entanglement witness.⁷⁴ In this work, we choose the typical polarization basis $\{|H\rangle, |V\rangle\}$ to investigate the coherence evolution of the quantum measurements, which is basis dependent. Our protocol also provides the flexibility to characterize the matrix components of the measurement operators in any basis of interest by adjusting the initial quantum state $\rho_s^{(j)}$ as well as the observables \hat{O}_B and $\hat{O}_A^{(k)}$ while other parts of the theoretical framework remain unchanged.

Our protocol can be extended to a high-dimensional QS in which the coherence information of the quantum measurement among specified base states is of interest. The conventional QDT typically requires d^2 informationally complete probe states chosen from at least $d + 1$ basis to globally reconstruct the POVM in a d -dimensional QS. Thus as the dimension d increases, the preparation of the probe states becomes an experimental challenge, and the computational complexity of the reconstruction algorithm is significantly increased. Both factors complicate the task of QDT for high-dimensional QSSs. In our scheme, the preparation of the initial states and the sequentially measured observables \hat{O}_B and $\hat{O}_A^{(k)}$ are simply involved in two bases, i.e., the representation basis $\{|a_j\rangle\}$ and its Fourier conjugate $\{|b\rangle\}$. The matrix components of the POVM can be directly inferred from the measurement results of the final MSs without resort to the reconstruction algorithm. When the matrix components are sparse in the measurement operators, our scheme can further simplify the characterization process. Therefore, the direct protocol also shows potential advantages over the conventional QDT in completely determining the POVM due to its better generalization to high-dimensional QSSs. In conclusion, by proposing a framework to directly and precisely measure the arbitrary single-matrix entry of the measurement operators, our results pave the way for both fully characterizing the quantum measurement and investigating the quantum properties of it.

6 Appendix: Dephasing and Phase Rotation of Quantum Measurements

6.1 Theoretical Derivation

A general POVM can be implemented through quantum walk with the unitary evolution \hat{U} of the QS at the position $x = 0$. After the quantum walk, the position $x = l$ corresponds to the POVM element

$$\hat{\Pi}_I = \text{Tr}_W[(|0\rangle\langle 0| \otimes \hat{I})\hat{U}^\dagger(|I\rangle\langle I| \otimes \hat{I})\hat{U}], \quad (13)$$

where $\text{Tr}_W[\cdot]$ denotes the partial trace in the walker position DOF. We implement the dephasing of the POVM $\{\hat{\Pi}_I\}$ by coupling the QS to the environment state ρ_E under the Hamiltonian $\hat{H}_{SE} = \frac{\epsilon}{2}\delta(t-t_0)\hat{C}\hat{\Omega}$ in which $\hat{C} = |a_j\rangle\langle a_j| - |a_k\rangle\langle a_k|$ and $\hat{\Omega}$ are the observables of the QS and the environment, respectively. By reducing the environment DOF, the measurement operator $\hat{\Pi}_I$ is transformed to $\hat{\Pi}_I^D = \text{Tr}_E[\hat{U}_{SE}^\dagger \hat{\Pi}_I \otimes \rho_E \hat{U}_{SE}]$. We can infer that the dephasing process only changes the related matrix components $E_{a_j a_k}^{(I)}$ to $E_{a_j a_k}^{(I),D} = E_{a_j a_k}^{(I)} \xi$ with the coefficient $\xi = \text{Tr}[\exp(-i\frac{\epsilon}{2}\hat{\Omega})\rho_E \exp(-i\frac{\epsilon}{2}\hat{\Omega})]$.

6.2 Experimental Calibration

To calibrate the relation between the coefficient ξ and the relative time delay $\epsilon = |t_H - t_V|$, we construct the setup shown in Fig. 5(a) in which both the HWPs are set to 22.5 deg. The photons in $|H\rangle$ enter the calibration setup resulting in the final state after the second HWP:

$$\rho^D = \frac{1+\xi}{2}|H\rangle\langle H| + \frac{1-\xi}{2}|V\rangle\langle V|. \quad (14)$$

Then ρ^D is projected to the basis $\{|H\rangle, |V\rangle\}$ with a PBD, obtaining the probabilities P_H and P_V . The parameter ξ is given by $\xi = P_H - P_V$. The relation between ξ and the relative time delay ϵ is shown in Fig. 5(b) in which we take ϵ from 0 to 260 times the wavelength ($\lambda = 830$ nm) and the red circled points are adopted for the experiment.

The liquid crystal imposes a relative phase ϕ_{lc} between $|H\rangle$ and $|V\rangle$ controlled by the voltage. Through the calibration setup in Fig. 5(a), the phase can be obtained by $\phi_{lc} = \arccos[2(P_H - P_V)]$. The calibration results of the relation between the phase ϕ_{lc} and the applied voltage are shown in Fig. 5(c). Here we adjust the voltages to 1.32 and 2.01 V, and the relative phases are $\sim 4\pi/5$ and $2\pi/5$.

Acknowledgments

This work was supported by the National Key Research and Development Program of China (Grant Nos. 2018YFA0306202 and 2017YFA0303703), National Natural Science Foundation of China (Grant Nos. 91836303, 61975077, 61490711, and 11690032), and Fundamental Research Funds for the Central Universities (Grant No. 020214380068). The authors declare no conflicts of interest.

Code, Data, and Materials Availability

The computer software code and data are available by connecting to the corresponding authors.

References

1. A. Ourjoumsev et al., "Generation of optical 'Schrödinger cats' from photon number states," *Nature* **448**(7155), 784–786 (2007).
2. E. Bimbard et al., "Quantum-optical state engineering up to the two-photon level," *Nat. Photonics* **4**(4), 243–247 (2010).
3. A. E. Ulanov et al., "Loss-tolerant state engineering for quantum-enhanced metrology via the reverse Hong–Ou–Mandel effect," *Nat. Commun.* **7**(1), 11925 (2016).
4. B. L. Higgins et al., "Entanglement-free Heisenberg-limited phase estimation," *Nature* **450**(7168), 393–396 (2007).
5. E. Knill, R. Laflamme, and G. J. Milburn, "A scheme for efficient quantum computation with linear optics," *Nature* **409**(6816), 46–52 (2001).
6. K. J. Resch et al., "Time-reversal and super-resolving phase measurements," *Phys. Rev. Lett.* **98**(22), 223601 (2007).
7. P. Kok et al., "Linear optical quantum computing with photonic qubits," *Rev. Mod. Phys.* **79**(1), 135–174 (2007).
8. A. Zhang et al., "Experimental test of contextuality in quantum and classical systems," *Phys. Rev. Lett.* **122**(8), 080401 (2019).
9. T. Li et al., "Experimental contextuality in classical light," *Sci. Rep.* **7**(1), 44467 (2017).
10. D. Frustaglia et al., "Classical physics and the bounds of quantum correlations," *Phys. Rev. Lett.* **116**(25), 250404 (2016).
11. M. Markiewicz et al., "From contextuality of a single photon to realism of an electromagnetic wave," *NPJ Quantum Inf.* **5**(1), 5 (2019).
12. S. Berg-Johansen et al., "Classically entangled optical beams for high-speed kinematic sensing," *Optica* **2**(10), 864–868 (2015).
13. D. Guzman-Silva et al., "Demonstration of local teleportation using classical entanglement," *Laser Photonics Rev.* **10**(2), 317–321 (2016).
14. B. Ndagano et al., "Characterizing quantum channels with non-separable states of classical light," *Nat. Phys.* **13**(4), 397–402 (2017).
15. A. Z. Goldberg et al., "Extremal quantum states," *AVS Quantum Sci.* **2**(4), 044701 (2020).
16. S. M. Barnett et al., "Retrodiction for quantum optical communications," *Phys. Rev. A* **62**(2), 022313 (2000).
17. D. T. Pegg, S. M. Barnett, and J. Jeffers, "Quantum retrodiction in open systems," *Phys. Rev. A* **66**(2), 022106 (2002).
18. T. Amri, J. Laurat, and C. Fabre, "Characterizing quantum properties of a measurement apparatus: insights from the retrodictive approach," *Phys. Rev. Lett.* **106**(2), 020502 (2011).
19. T. Theurer et al., "Quantifying operations with an application to coherence," *Phys. Rev. Lett.* **122**(19), 190405 (2019).
20. V. Cimini et al., "Measuring coherence of quantum measurements," *Phys. Rev. Res.* **1**(3), 033020 (2019).
21. F. Bischof, H. Kampermann, and D. Bruß, "Resource theory of coherence based on positive-operator-valued measures," *Phys. Rev. Lett.* **123**(11), 110402 (2019).
22. T. Guff et al., "A resource theory of quantum measurements," *J. Phys. A: Math. Theor.* **54**(22), 225301 (2021).
23. H. Xu et al., "Experimental quantification of coherence of a tunable quantum detector," *Phys. Rev. Lett.* **125**(6), 060404 (2020).
24. J. Lundeen et al., "Tomography of quantum detectors," *Nat. Phys.* **5**(1), 27–30 (2009).
25. G. M. D'Ariano, L. Maccone, and P. L. Presti, "Quantum calibration of measurement instrumentation," *Phys. Rev. Lett.* **93**(25), 250407 (2004).
26. A. Luis and L. L. Sánchez-Soto, "Complete characterization of arbitrary quantum measurement processes," *Phys. Rev. Lett.* **83**(18), 3573–3576 (1999).
27. J. Fiurášek, "Maximum-likelihood estimation of quantum measurement," *Phys. Rev. A* **64**(2), 024102 (2001).
28. V. d'Auria et al., "Quantum decoherence of single-photon counters," *Phys. Rev. Lett.* **107**(5), 050504 (2011).
29. A. Feito et al., "Measuring measurement: theory and practice," *New J. Phys.* **11**(9), 093038 (2009).
30. H. B. Coldenstrod-Ronge et al., "A proposed testbed for detector tomography," *J. Mod. Opt.* **56**(2–3), 432–441 (2009).
31. G. Brida et al., "Quantum characterization of superconducting photon counters," *New J. Phys.* **14**(8), 085001 (2012).
32. M. K. Akhlaghi, A. H. Majedi, and J. S. Lundeen, "Nonlinearity in single photon detection: modeling and quantum tomography," *Opt. Express* **19**(22), 21305–21312 (2011).

33. A. Worsley et al., “Absolute efficiency estimation of photon-number-resolving detectors using twin beams,” *Opt. Express* **17**(6), 4397–4412 (2009).
34. D. Mayers and A. Yao, “Quantum cryptography with imperfect apparatus,” in *Proc. 39th Annu. Symp. Found. Comput. Sci.*, IEEE, pp. 503–509 (1998).
35. E. S. Gómez et al., “Device-independent certification of a non-projective qubit measurement,” *Phys. Rev. Lett.* **117**(26), 260401 (2016).
36. W.-H. Zhang et al., “Experimentally robust self-testing for bipartite and tripartite entangled states,” *Phys. Rev. Lett.* **121**(24), 240402 (2018).
37. A. Tavakoli et al., “Self-testing quantum states and measurements in the prepare-and-measure scenario,” *Phys. Rev. A* **98**(6), 062307 (2018).
38. J. Řeháček, D. Mogilevtsev, and Z. Hradil, “Operational tomography: fitting of data patterns,” *Phys. Rev. Lett.* **105**(1), 010402 (2010).
39. D. Mogilevtsev et al., “Data pattern tomography: reconstruction with an unknown apparatus,” *New J. Phys.* **15**(2), 025038 (2013).
40. L. Zhang et al., “Mapping coherence in measurement via full quantum tomography of a hybrid optical detector,” *Nat. Photonics* **6**(6), 364–368 (2012).
41. J. Renema et al., “Experimental test of theories of the detection mechanism in a nanowire superconducting single photon detector,” *Phys. Rev. Lett.* **112**(11), 117604 (2014).
42. J. S. Lundeen et al., “Direct measurement of the quantum wavefunction,” *Nature* **474**(7350), 188–191 (2011).
43. M. Malik et al., “Direct measurement of a 27-dimensional orbital-angular-momentum state vector,” *Nat. Commun.* **5**(1), 3115 (2014).
44. G. A. Howland, D. J. Lum, and J. C. Howell, “Compressive wavefront sensing with weak values,” *Opt. Express* **22**(16), 18870–18880 (2014).
45. M. Mirhosseini et al., “Compressive direct measurement of the quantum wave function,” *Phys. Rev. Lett.* **113**(9), 090402 (2014).
46. S. H. Knarr et al., “Compressive direct imaging of a billion-dimensional optical phase space,” *Phys. Rev. A* **98**(2), 023854 (2018).
47. Z. Shi et al., “Scan-free direct measurement of an extremely high-dimensional photonic state,” *Optica* **2**(4), 388–392 (2015).
48. K. Ogawa et al., “A framework for measuring weak values without weak interactions and its diagrammatic representation,” *New J. Phys.* **21**(4), 043013 (2019).
49. K. Ogawa et al., “Direct measurement of ultrafast temporal wavefunctions,” *Opt. Express* **29**(13), 19403–19416 (2021).
50. Y. Zhou et al., “Direct tomography of high-dimensional density matrices for general quantum states of photons,” *Phys. Rev. Lett.* **127**(4), 040402 (2021).
51. M. Yang et al., “Zonal reconstruction of photonic wavefunction via momentum weak measurement,” *Laser Photonics Rev.* **14**(5), 1900251 (2020).
52. J. Z. Salvail et al., “Full characterization of polarization states of light via direct measurement,” *Nat. Photonics* **7**(4), 316–321 (2013).
53. C. Bamber and J. S. Lundeen, “Observing Dirac’s classical phase space analog to the quantum state,” *Phys. Rev. Lett.* **112**(7), 070405 (2014).
54. J. S. Lundeen and C. Bamber, “Procedure for direct measurement of general quantum states using weak measurement,” *Phys. Rev. Lett.* **108**(7), 070402 (2012).
55. G. S. Thekkadath et al., “Direct measurement of the density matrix of a quantum system,” *Phys. Rev. Lett.* **117**(12), 120401 (2016).
56. S. Wu, “State tomography via weak measurements,” *Sci. Rep.* **3**(1), 1193 (2013).
57. C. Ren, Y. Wang, and J. Du, “Efficient direct measurement of arbitrary quantum systems via weak measurement,” *Phys. Rev. Appl.* **12**(1), 014045 (2019).
58. W.-W. Pan et al., “Direct measurement of a nonlocal entangled quantum state,” *Phys. Rev. Lett.* **123**(15), 150402 (2019).
59. Y. Kim et al., “Direct quantum process tomography via measuring sequential weak values of incompatible observables,” *Nat. Commun.* **9**(1), 192 (2018).
60. L. Xu et al., “Direct characterization of quantum measurements using weak values,” *Phys. Rev. Lett.* **127**(18), 180401 (2021).
61. P. Zou, Z.-M. Zhang, and W. Song, “Direct measurement of general quantum states using strong measurement,” *Phys. Rev. A* **91**(5), 052109 (2015).
62. G. Vallone and D. Dequal, “Strong measurements give a better direct measurement of the quantum wave function,” *Phys. Rev. Lett.* **116**(4), 040502 (2016).
63. Y.-X. Zhang, S. Wu, and Z.-B. Chen, “Coupling-deformed pointer observables and weak values,” *Phys. Rev. A* **93**(3), 032128 (2016).
64. X. Zhu, Y.-X. Zhang, and S. Wu, “Direct state reconstruction with coupling-deformed pointer observables,” *Phys. Rev. A* **93**(6), 062304 (2016).
65. T. Denkmayr et al., “Experimental demonstration of direct path state characterization by strongly measuring weak values in a matter-wave interferometer,” *Phys. Rev. Lett.* **118**(1), 010402 (2017).
66. L. Calderaro et al., “Direct reconstruction of the quantum density matrix by strong measurements,” *Phys. Rev. Lett.* **121**(23), 230501 (2018).
67. X. Zhu et al., “Hybrid direct state tomography by weak value,” <https://arxiv.org/abs/1909.02461> (2019).
68. C.-R. Zhang et al., “Direct measurement of the two-dimensional spatial quantum wave function via strong measurements,” *Phys. Rev. A* **101**(1), 012119 (2020).
69. M.-C. Chen et al., “Directly measuring a multiparticle quantum wave function via quantum teleportation,” *Phys. Rev. Lett.* **127**(3), 030402 (2021).
70. J. A. Gross et al., “Novelty, efficacy, and significance of weak measurements for quantum tomography,” *Phys. Rev. A* **92**(6), 062133 (2015).
71. E. Haapasalo, P. Lahti, and J. Schultz, “Weak versus approximate values in quantum state determination,” *Phys. Rev. A* **84**(5), 052107 (2011).
72. Z. Bian et al., “Realization of single-qubit positive-operator-valued measurement via a one-dimensional photonic quantum walk,” *Phys. Rev. Lett.* **114**(20), 203602 (2015).
73. D. Brivio et al., “Experimental estimation of one-parameter qubit gates in the presence of phase diffusion,” *Phys. Rev. A* **81**(1), 012305 (2010).
74. R. Horodecki et al., “Quantum entanglement,” *Rev. Mod. Phys.* **81**(2), 865–942 (2009).

Liang Xu received his BS degree in physics of materials and his PhD in optics engineering from Nanjing University in 2014 and 2020, respectively. He is a postdoc fellow at Zhejiang Laboratory. His current research interests include weak measurement, quantum metrology, and quantum tomography.

Huichao Xu received his BS and MS degrees in telecommunication from the University of Jiamusi and University of Liverpool in 2009 and 2011, respectively, and his PhD in quantum optics from Nanjing University in 2020. He is an assistant researcher at Nanjing University. His current research interests include quantum state generation and quantum detectors.

Jie Xie received his BS degree in applied physics from Southwest Jiaotong University. He is a PhD student at the School of Physics of Nanjing University. His current research interests include quantum simulation in linear photonics.

Hui Li received his BE degree in optoelectronic information science and engineering from China University of Petroleum. He is a PhD student at the College of Engineering and Applied Sciences of Nanjing University.

His current research interests include quantum walk and quantum fluctuation.

Lin Zhou received his BS degree in physics of materials in 2020. He is a graduate student at Nanjing University. His current research interests include quantum metrology, quantum tomography and light manipulation.

Feixiang Xu received his BS degree in physics from Nanchang University in 2016, and his PhD in optics engineering from Nanjing University in 2021. He is now an assistant researcher at Nanjing University. His current

research interests include the resource theory of quantum coherence, quantum imaging and quantum tomography.

Lijian Zhang received his BS and MS degrees in electrical engineering from Peking University in 2000 and 2003, respectively, and his PhD in physics from the University of Oxford in 2009. He is a professor at the College of Engineering and Applied Sciences of Nanjing University. He is the author of more than 50 journal papers and two book chapters. His current research interests include quantum optics and quantum information processing.